Coalescent-based species delimitation meets deep learning: Insights from a highly fragmented cactus system

MANOLO F. PEREZ[1,2,¥], ISABEL A. S. BONATELLI[1,3,,¥], MONIQUE ROMEIRO-BRITO[1], FERNANDO F. FRANCO[1], NIGEL P. TAYLOR[4], DANIELA C. ZAPPI[5], EVANDRO M. MORAES[1,*]

[1]*Departamento de Biologia, Universidade Federal de São Carlos, Rodovia João Leme dos Santos km 110, Sorocaba, SP, 18052780, Brazil;*

[2]*Departamento de Genética e Evolução, Universidade Federal de São Carlos, Rodovia Washington Luiz km 235, C.P. 676, São Carlos, SP, 13565905, Brazil;*

[3]*Departamento de Ecologia e Biologia Evolutiva, Universidade Federal de São Paulo, Diadema, SP 09972-270, Brazil;*

[4]*University of Gibraltar, Gibraltar Botanic Gardens Campus, The Alameda, PO Box 843, Gibraltar;*

[5]*Programa de Pós Graduação em Botânica, Instituto de Ciências Biológicas, Universidade de Brasília, PO Box 04457, Brasília, DF, 70910970, Brazil.*

[¥] *Manolo F. Perez and Isabel A. S. Bonatelli contributed equally to this article.*

* *Correspondence to be sent to Departamento de Biologia, Universidade Federal de São Carlos, Rodovia João Leme dos Santos km 110, Sorocaba, SP, 18052780, Brazil;*

E-mail: emarsola@ufscar.br

Abstract. - Delimiting species boundaries is a major goal in evolutionary biology. An increasing body of literature has focused on the challenges of investigating cryptic diversity within complex evolutionary scenarios of speciation, including gene flow and demographic fluctuations. New methods based on model selection, such as approximate Bayesian computation, approximate likelihood, and machine learning approaches, are promising tools arising in this field. Here, we introduce a framework for species delimitation using the multispecies coalescent model coupled with a deep learning algorithm based on

convolutional neural networks (CNNs). We compared this strategy with a similar ABC approach. We applied both methods to test species boundary hypotheses based on current and previous taxonomic delimitations as well as genetic data (sequences from 41 loci) in *Pilosocereus aurisetus*, a cactus species with a sky-island distribution and taxonomic uncertainty. To validate our proposed method, we also applied the same strategy on sequence data from widely accepted species from the genus *Drosophila*. The results show that our CNN approach has high capacity to distinguish among the simulated species delimitation scenarios, with higher accuracy than the ABC procedure. For *Pilosocereus*, the delimitation hypothesis based on a splitter taxonomic arrangement without migration showed the highest probability in both CNN and ABC approaches. The splits observed within *P. aurisetus* agree with previous taxonomic conjectures considering more taxonomic entities within currently accepted species. Our results highlight the cryptic diversity within *P. aurisetus* and show that CNNs are a promising approach for distinguishing divergent and complex evolutionary histories, even outperforming the accuracy of other model-based approaches such as ABC.

Keywords: Species delimitation, fragmented systems, recent diversification, deep learning, Convolutional Neural Networks, Approximate Bayesian Computation

INTRODUCTION

Recognizing species boundaries has long been a major challenge for biologists. The major difficulty is to some degree related to the numerous existing species concepts. The use of distinct concepts can lead to different strategies for identifying species boundaries in empirical datasets (de Queiroz 2007; Carstens et al. 2013). However, different species concepts can be considered elements related to diverse properties that are associated with the dynamics of the speciation continuum. After the proposal of the unified species concept

(Queiroz, 2007), the roles of species concepts as a theory and species delimitation as a methodology become apparent. The view of species as independent segments of a metapopulation indicated lineage independence as the only criterion necessary for delimiting species boundaries, avoiding any disagreement purely related to the species concept.

Selecting a suitable approach for species delimitation has been difficult, especially in species complexes (Pinheiro et al. 2018). Identifying discontinuities among incipient stages of divergence, such as those found in these systems, demands great effort and a multidisciplinary approach to assess different sources of evidence supporting species limits (Carstens et al. 2013). In this context, estimates based on independent sources of data such as morphology, cytogenetics, anatomy, ecology, and genetics have been used to achieve a better resolution in species delimitation (Domingos et al. 2014; Alvarado-Sizzo et al. 2018; Denham et al. 2019). Some of these traits, such as phenotypes and geographic distributions, can be a starting point for hypotheses about species circumscriptions (Solís-Lemus et al. 2015; Luo et al. 2018).

Species delimitation methods based on multilocus data and the multispecies coalescent model (MSC) compare the probability of species trees with different numbers of operational taxonomic units (OTUs) to identify optimal partitions for the data (Ence and Carstens 2011). Highly fragmented systems impose potential caveats on such methods, potentially resulting in the oversplit of existing diversity, and thus, highly subdivided entities (Sukumaran and Knowles 2017). Jackson et al. (2017) proposed the incorporation of the genealogical divergence index (*gdi*) as an attempt to reduce the delimitation of population structure, instead of species limits. Furthermore, the developers of the bayesian delimitation method implemented in BPP (Yang and Rannala 2014) described an approach to integrate *gdi* on the outputs of their software and showed that such a strategy was efficient in mitigating the effect of over splitting (Leaché et al. 2018). However, a number of concerns on the use of *gdi* have

been raised. For instance, a large interval of *gdi* values (0.2 to 0.7) that corresponds to a 'grey zone' where delimitation is ambiguous, and datasets containing putative species with population sizes very different or extremely small (Rannala and Yang 2020).

Model selection methods using simulated datasets under competing delimitation hypotheses are a promising tool for taxa that have potentially experienced a complex evolutionary history, including recurrent gene flow and demographic fluctuations. These methods also allow us to easily test for different assignments and topologies of the analyzed samples into populations/species, a procedure that is not straightforward with other approaches (but see Leaché et al. 2014). Examples of such approaches include approximate Bayesian computation (ABC; Camargo et al. 2012), approximate likelihood analysis (Morales et al. 2017), machine learning coupled with ABC (Smith and Carstens 2020) and machine learning methods based on summary statistics (SuSt) (Pei et al. 2018). Among them, the ABC represents a class of flexible likelihood-free algorithms for performing Bayesian inference (Beaumont et al. 2002). The principle behind the method relies on the massive simulation of genetic data using parameter values drawn from a prior distribution, followed by the calculation of SuSt for each simulation. SuSt are values generated from the raw genetic data, which are expected to capture important information to differentiate among the simulated models. Simulations that produce genetic variation patterns (SuSt) close to the observed data are retained to form an approximate sample from the posterior distribution.

A recently developed approach for demographic model selection, based on deep learning image classification, uses convolutional neural networks (CNNs) to retrieve as much information as possible from genetic datasets by converting them to images without requiring user-specified SuSt (Flagel et al. 2019). Simulations have shown that CNNs maximize the use of available information from the data and increase the ability to distinguish divergent evolutionary histories, frequently overcoming the limitations of traditional approaches (Flagel

102 et al. 2019). Despite the recent use of CNNs in population genetics (Flagel et al. 2019;
103 Sanchez et al. 2020) and phylogeography (Souza et al. 2019; Oliveira et al. 2020; da Fonseca
104 et al. 2020), this approach has not previously been tested in the context of species
105 delimitation using genetic data.

106 Here, we introduce an approach for species delimitation that combines the use of MSC-
107 based methods with model selection via CNN. We compared our model selection method
108 with ABC to evaluate distinct species delimitation hypotheses in the cactus *Pilosocereus*
109 *aurisetus.* We chose this taxon because (1) it presents a controversial taxonomy, and (2) it has
110 a highly fragmented geographical distribution, comparable to other sky-island systems,
111 imposing recognized difficulties upon MSC-based methods (Leaché et al. 2018).

112 To gain better insights into the species limits in *P. aurisetus,* we used the following
113 protocol (Fig. 1): (1) apply the MSC approach implemented in BPP (Yang and Rannala 2014)
114 with sequence data and OTUs based on sampling localities, (2) apply the *gdi* index to the
115 BPP results, to obtain a hypothesis less prone to oversplitting, (3) simulate data under the
116 obtained BPP results (with and without *gdi*) and for each taxonomic hypothesis, with and
117 without gene flow among lineages (this step requires some previous knowledge about the
118 study group, such as divergence times, effective population size, and number of migrants per
119 generation, when applicable), (3) transform the simulated data into binary images, defining
120 the major and minor state for each site, (4) train a CNN to recognize simulations generated
121 from each model, (5) evaluate the accuracy of the trained CNN in comparison to an ABC
122 approach, by using cross-validation tests based on simulated data (i.e. independent
123 simulations not evaluated before), and (6) predict model probability with the trained network
124 (CNN) or by approximating the posterior (ABC). We also validated our method by following
125 this same procedure using a recently published dataset from two *Drosophila* species pairs

(Campillo et al. 2020), which have information about pre- and postzygotic reproductive isolation and do not have controversial taxonomy.

MATERIAL AND METHODS

The Studied System

The taxon *P. aurisetus* is a puzzling system regarding species delimitation. The taxonomy of *P. aurisetus* has been unstable over the years, which is a common attribute in the family Cactaceae, probably related to the absence of clear diagnostic characters for some groups due to convergent and parallel evolution (Hernández-Hernández et al. 2011; Copetti et al. 2017). The morphological variation observed within this taxon has led to repeated taxonomic evaluations, with species and subspecies being recurrently synonymized and re-established (Zappi, 1994; Taylor and Zappi, 2004; Hunt et al., 2006). Another complicating issue is the naturally fragmented distribution of *P. aurisetus*. The taxon is associated with the Espinhaço Mountain Range campo rupestre landscapes in eastern Brazil, occurring on mountaintops separated by valleys and lowland vegetation (Fig. 2). In line with this sky-island distribution, *P. aurisetus* shows high intraspecific genetic structure (Bonatelli et al. 2014; Perez et al. 2016a, b). Currently, two subspecies are recognized based on differences in the size and diameter of stems and the color and density of hairs on flower-bearing areoles: the more widespread *P. aurisetus* subsp. *aurisetus* (Werderm.) Byles & Rowley, and *P. aurisetus* subsp. *aurilanatus* (Ritter) Zappi, which occurs as few populations restricted to a disjunct mountain (Serra do Cabral) west of the Espinhaço Mountain Range. We also included in our study plants from three heterotypic synonyms of *P. aurisetus* subsp. *aurisetus* (Fig. S1): *P. aurisetus* subsp. *densilanatus* (Ritter) Braun & Esteves, located in the easternmost populations from the Serra Negra Mountains and distinguished by their densely wooly stems, reaching up to 4 cm diameter; *P. aurisetus* subsp. *supthutianus* (Braun) Braun & Esteves, a northern outlier of the species that also present densely hairy stems, which can

151 reach more than 5 cm diameter; and *P. aurisetus* subsp. *werdermannianus* (Buining &
152 Brederoo) Braun & Esteves, located in the central populations and showing more slender
153 stems, fewer ribs and sometimes green epidermis.
154
155 *Sampling and DNA extraction*
156 We sampled four individuals of *P. aurisetus* in each of nine localities in eastern Brazil,
157 totaling 36 sampled individuals and covering the entire known distribution of the species.
158 Hereafter, we refer to these sampled localities as populations justified by the clear limits of
159 the *P. aurisetus* habitat patches and the marked genetic structure in this taxon (Bonatelli et al.
160 2014). This sampling included representatives of all accepted and synonymized taxa
161 mentioned above (Fig. 2; Table 1). Root tissue was stored in silica gel and then transferred to
162 a -80°C freezer until DNA extraction. We maintained a distance of approximately 10 m
163 between sampled individuals to avoid collecting clones. Total DNA was extracted using the
164 Extract All kit (Applied Biosystems) and purified with 95% ethanol and 3 M sodium acetate
165 buffer. The DNA concentration was measured with a Qubit fluorometer (Invitrogen).
166
167 *Microfluidic PCR and sequencing*
168 Massive parallel target amplification of 41 loci in 36 samples was carried out in
169 microfluidic PCR reactors (Access Array System, Fluidigm). The selected loci included 26
170 anonymous nuclear markers developed for *P. aurisetus* (Perez et al. 2016c) and another five
171 nuclear, eight plastid and two mitochondrial genic regions selected from the available data in
172 GenBank (Supplementary Table S1). Development of these new markers was based on
173 available sequences from Cactaceae or from other related plant family species to detect
174 conserved regions for primer design. All primers were developed with PRIMER3 v4.0.0
175 (Untergrasser et al. 2012), with parameters suggested by the Fluidigm Assay Design Group

176 as follows: primer size from 18–23 bases, annealing temperature between 59°C and 61°C,
177 maximum poli-X of 3. The selected markers were synthesized according to Fluidigm
178 specifications and applied to a single 48×48 access array chip with reactions performed
179 according to the manufacturer's protocol. The obtained PCR products were pooled and
180 purified with 0.6X AMPure beads (Agencourt). The quality and amplification range were
181 visualized in a BioAnalyzer, and the concentration was estimated via real-time PCR using
182 KAPA qPCR (Kapa Biosystems). The samples were subjected to a MiSeq (Illumina) 300 bp
183 paired-end run along with 156 other samples from other projects.
184 After sequencing, a first filtering step was performed with cutadapt (Martin 2011), excluding
185 sequences smaller than 60 bp and removing 3' bases with a PHRED score <Q22. PHRED
186 quality for all reads was then visualized in FastQC
187 (http://www.bioinformatics.bbsrc.ac.uk/projects/fastqc) and graphically compiled in MultiQC
188 (http://multiqc.info/). Reference sequences for each marker were generated from the
189 alignments used to design the primers. Mapping reads for each marker was performed with
190 BWA-MEM (Li 2013), which is suited for pair-end long reads with indels, while SAMtools
191 (Li et al. 2009) was used to retain only sequences that were mapped with high fidelity. SNP
192 calling was carried out with GATK (McKenna et al. 2010) by transforming low-quality bases
193 in missing data, identifying possible indels with realignment, applying polymorphism filters
194 for quality and coverage, and generating FASTA files for each sample. To confirm the
195 obtained polymorphisms, each detected SNP was then mapped against reference files for
196 each marker that were built from reads from each analyzed sample. The phasing of SNPs in
197 nuclear markers was achieved with a Python script, modified from Harvey et al. (2016). The
198 aligned sequences from each marker were obtained with MAFFT v.7 (Katoh and Standley
199 2013) with default parameters. Recombination within each marker was tested with the DSS
200 method (McGuire and Wright 2000) implemented in TOPALi v2 (Milne et al. 2008) and

201 topological incongruences were tested in KDETrees (Weyenberg et al. 2014). The most likely
202 substitution model for each locus was obtained with PartitionFinder v.1.1.1 (Lanfear et al.
203 2012).
204
205 *Species Tree and Coalescent Delimitation*
206 The phylogenetic relationships among populations were recovered with a species tree in
207 BEAST v2.1.3 (Bouckaert et al. 2014), assigning the sequences from each population to a
208 single OTU. For all markers, we used the selected substitution model (Table S1) and a
209 Relaxed clock Log-Normal, with the mean sampled from a broad lognormal distribution
210 (according to Perez et al. 2016b). We performed three runs with 5 x 10^8 MCMC iterations
211 each, sampling trees every 10^4 generations with 75% burn-in. Convergence was observed in
212 TRACER 1.6 (Rambaut et al. 2014) and a Maximum Clade Credibility (MCC) tree with
213 median heights was obtained in TreeAnnotator (Drummond and Rambaut 2007).
214 We used the obtained species tree topology and the genomic sequences obtained from
215 microfluidic PCR as input to test the species limits in *P. aurisetus* with the method
216 implemented in BPP v3.4 (Yang and Rannala 2014). For this analysis, we concatenated all
217 mitochondrial (*cox1* and *cox2*) and chloroplast (*atpB-rbcL*, *petL-psbE* and *rpl16*) markers.
218 The BPP method uses a reversible jump Bayesian (rjMCMC) framework to estimate the
219 posterior probability of existence at each node of the phylogeny. To ensure convergence, five
220 independent runs were performed to estimate the best delimitation scheme, with parameters
221 selected according to the values suggested by Leaché et al. (2018) combined with previous
222 estimates for the species from Perez et al. (2016a). θ and τ priors followed an inverse gamma
223 (IG) distribution with α=3 and a β of 0.01 and 0.002, respectively (hereafter BPP 'specific
224 prior values'). We evaluated the potential effect of priors in the delimitation results by also
225 performing the same number of runs with broad prior values $\theta \sim$ IG(3, 0.002) and $\tau \sim$ IG(3,

226 0.03) as suggested in the BPP manual (hereafter 'diffuse prior values'). We considered a node
227 as valid only if both analyses support its existence with a posterior probability (PP) of 0.99 or
228 higher. The runs were carried out for 10^5 iterations sampled every five steps after discarding
229 the first 10^4 iterations as burn-in. The obtained delimitations were mapped to the tips of the
230 species tree topology. As a more conservative alternative, we also evaluated our BPP results
231 using the *gdi* index, as suggested by Leaché et al. (2018). We considered the threshold values
232 suggested by Jackson et al. (2017) and Leaché et al. (2018), in which pairwise *gdi* values
233 smaller than 0.2 indicate a single species and above 0.7, two species.
234
235 *Comparing Delimitation Hypotheses with Deep Learning and ABC*
236 We adopted an integrative approach to establish putative species limits by considering
237 information on *P. aurisetus* from different sources and analyses, as suggested by Carstens et
238 al. (2013). For that, we compared the two delimitation hypotheses generated by the BPP
239 results (with and without the *gdi* index), as well as two morphological hypotheses based on
240 one lumper and one splitter taxonomic arrangement (Table 1; Fig. 1). The genetic hypotheses,
241 based on the BPP results, were composed of one species when *gdi* was considered and four
242 species when it was not incorporated (see results below); the 'splitter' morphological
243 hypothesis, considering both currently accepted and previously synonymized taxa, was
244 composed of four species; and the 'lumper' morphological hypothesis, considering only the
245 currently recognized subspecies, was composed of two species (Hunt et al. 2006). To test
246 these competing delimitation hypotheses, we considered scenarios including the number of
247 species and the potential migration between the delimited entities. Therefore, seven scenarios
248 (Fig. 1) were tested: (1) 'splitter', (2) 'splitter' combined with migration, (3) 'lumper', (4)
249 'lumper' with migration, (5) BPP combined with *gdi* (BPP_GDI), (6) BPP without *gdi*
250 (BPP_noGDI), and (7) BPP_noGDI with migration. As the BPP_GDI scenario consists of a

single species, an additional model including migration was not necessary. We performed model comparison using both a deep learning approach based on CNN and a regular ABC method. For these two strategies, we simulated genetic datasets under each scenario with a modified version of the scripts from Perez et al. (2016a). To simplify our simulations and avoid using an overly heterogeneous dataset, we included only nuclear markers and simulated data mirroring sample sizes with the same number of segregating sites per loci of our empirical dataset. For the deep learning approach, the simulated data were converted to images that were used to train a CNN to recognize simulations generated by different scenarios (for details on the simulation and training procedure, see Supplementary File 1). The comparison of delimitation scenarios using regular ABC analysis (Fig. 1) was performed following the approach of Perez et al. (2016a) with simulations conducted under the same conditions used for the CNN (details in Supplementary File 1).

To validate our newly proposed deep learning method for species delimitation, we also carried out the same analyses using a dataset recently published by Campillo et al. (2020). These authors compared the results of reproductive isolation and coalescent-based (BPP) delimitation methods to infer species boundaries in several species pairs of the genus *Drosophila*, a classic model system in speciation research. We focused our approach on data from two species pairs of the Melanogaster group: *D. melanogaster* - *D. sechellia* and *D. melanogaster* - *D. simulans*. We chose these species because they are widely accepted and corroborated by both BPP and reproductive isolation metrics (Campillo et al. 2020). Furthermore, while the *D. melanogaster* - *D. sechellia* pair is allopatric, the *D. melanogaster* - *D. simulans* pair is sympatric, allowing us to explore whether geographic context might affect our ability to identify these species. Therefore, we tested a model with all specimens belonging to the same species against a model in which the specimens were divided into two species, which was the expected outcome according to the current classification. Again, our

simulations were based on empirical sample sizes and the number of segregating sites (details in Supplementary File 1), with priors based on the values suggested by Campillo et al. (2020).

RESULTS

Microfluidic PCR and sequencing

Four markers showed no amplification in any sample (*PaANL*_46, *petA*, *rpS16*, and *ycf1*). To further minimize missing data and ensure that at least one individual was sequenced from each population, we discarded 16 loci (*PaANL*_8, *PaANL*_10, *PaANL*_50, *PaANL*_82, *PaANL*_123, *PaANL*_134, *PaANL*_142, *PaANL*_155, *PaANL*_160, *PaANL*_187, *PaANL*_196, *its2*, *ppc*, *nhx1*, *psbA-psbB*, *psbC*). No recombination was detected at any of the remaining loci, but kdetrees result suggested an incongruent topology in the *isi1* marker, which was removed. Therefore, the final dataset included 20 markers that were considered in the subsequent analyses for *P. aurisetus* (*PaANL*_15, *PaANL*_17, *PaANL*_28, *PaANL*_35, *PaANL*_80, *PaANL*_87, *PaANL*_96, *PaANL*_126, *PaANL*_140, *PaANL*_147, *PaANL*_164, *PaANL*_165, *PaANL*_182, *PaANL*_205, *apk1*, *atpB-rbcL*, *petL-psbE*, *rpl16*, *cox1* and *cox2*), with a total of 8,908 bp.

Species Tree and Coalescent Delimitation

The species tree recovered most nodes with high support, especially the ones defining previously and currently valid subspecies (Fig. 3). Population JFE of *P. aurisetus* subsp. *aurilanatus* was the most external clade. Other populations were arranged in two subclades. One of them contained populations in the center (INA and MEN, previously classified as *P. a.* subsp. *werdermannianus*; ITA and PMN, formerly *P. a.* subsp. *densilanatus*) and south (COC)

300 of the *P. a.* subsp. *aurisetus* distribution. The second subclade contained populations from
301 northern distribution (EDB, BOV and ODA, formerly classified as *P. a.* subsp. *supthutianus*).
302 All BPP runs under each prior set showed the same results, therefore we provided the
303 mean posterior probability of each node in Fig. 3. Results with 'specific' and 'diffuse' priors
304 were similar, though the latter was less splitter. The congruent delimited species were *P. a.*
305 subsp. *aurisetus* (COC), *P. a.* subsp. *werdermannianus* (EDB, BOV and ODA) and the
306 currently recognized subspecies *P. aurisetus* subsp. *aurilanatus* (JFE). The only exception
307 was for the node separating the population ODA from the remaining *P. a.* subsp.
308 *supthutianus* populations (BOV and EDB), which was validated (PP=1) only in the 'specific'
309 but not (PP=0.95) in the 'diffuse' prior set. To be conservative, we decided to collapse this
310 node, considering all populations once recognized as *P. a.* subsp. *supthutianus* as a single
311 unit. Therefore, BPP resulted in four delimited species, that coincided with the 'splitter'
312 hypothesis, except for the OTUs composed by populations once recognized as *P. a.* subsp.
313 *werdermannianus* and *P. a.* subsp. *densilanatus*, which were collapsed (Fig. 3). When we
314 analyzed our BPP results with the *gdi* index, all estimates were below 0.7 and only three (*P.*
315 *aurisetus* subsp. *aurilanatus* - JFE; *P. a.* subsp. *aurisetus* - COC; and *P. a.* subsp.
316 *supthutianus* - ODA, BOV and EDB) had values between 0.2 and 0.7 (Fig. S2). Therefore, to
317 be conservative, we decided to collapse all populations in a single species for this hypothesis.
318

319 *Delimitation Hypotheses Comparison*

320 After 250 epochs, our CNN showed accuracies of 96.78% and 92.71% for the training
321 and validation sets, respectively. Some degree of overfitting was observed when we plotted
322 the accuracy of the training and validation sets throughout the epochs. However, this effect
323 decreased as the number of evaluated simulations increased (Fig. S3). Our cross-validation
324 procedure, using a test set of simulations not evaluated during training, also showed that

325 increasing the number of simulations resulted in accuracy improvement for all models (Fig.
326 4). It was also possible to observe that CNN presented a higher proportion of simulations that
327 were correctly predicted in relation to their generating model than the ABC results, with all
328 models being correctly assigned with more than 85% accuracy when 10,000 simulations per
329 model were used (Fig. 4 and S4). The percentages of correct predictions with the ABC
330 approach were all higher than 70% when 10,000 simulations per model were used, except for
331 the models with more delimited species that showed ~50% accuracy (Fig. 4). These two types
332 of models with lower accuracy in the ABC analysis ('splitter' and 'BPP_noGDI') showed the
333 most confusion with each other (Fig. S4). When the empirical data were submitted to the
334 trained CNN, the 'splitter' hypothesis was selected with a softmax probability of 99.8%
335 (Table 2). Our CNN approach showed consistent results, selecting the same delimitation
336 scenario even when the order of SNPs was shuffled (Supplementary File 1).The ABC
337 approach showed similar results, also recovering the 'splitter' hypothesis (PP=0.994). These
338 results are in agreement with what is observed when we plot the simulated and empirical
339 genotypes with a PCA (Fig. S5), showing that the empirical data are located inside the cloud
340 of simulations from the 'splitter' model .

341 The *Drosophila* dataset also pointed to a higher accuracy of CNN over ABC. The
342 cross-validation tests indicate a correct assignment of CNN simulations just above 78% and
343 81% in the *D. melanogaster-D simulans* and *D. melanogaster-D. sechellia* pairs, respectively
344 (Fig. S4). The accuracy of ABC was lower, reaching values slightly higher than 70% and
345 65% for the same species pairs (Fig. S4). When the empirical data were used, both methods
346 supported the hypothesis of two species for the *D. melanogaster-D simulans* pair, showing a
347 probability of 99.2% in CNN and 98.2% for ABC. In *D. melanogaster-D. sechellia,* the CNN
348 pointed to two species with a probability of 94.9%, while the ABC suggested a single species
349 with 89.4% PP (Table 2).

350

351 DISCUSSION

352 *Deep learning in coalescent-based species delimitation*

353 The advantages of the simulation approaches adopted here (CNN and ABC) over
354 explicit statistical methods are that they allow testing models with complex demographic
355 scenarios, such as migration events or size fluctuations. In addition to this use, these
356 approaches allow to easily apply different assignments of samples into OTUs (but see Leaché
357 et al. 2014) and even compare hypotheses relying on distinct topologies. Our comparison of
358 these two approximate approaches suggests that the deep learning approach (CNN) showed a
359 higher capacity to distinguish among the simulated demographic scenarios, outperforming the
360 ABC procedure (Fig. 4 and S4). It is important to highlight that CNN achieved this
361 performance with longer, though not impeditive, running times (~21 minutes in a Nvidia
362 K80 GPU with an Intel Xeon 2.30GHz CPU) than ABC (~1 minute in an Intel Core i7
363 2.9GHz CPU). The results from the *Drosophila* dataset also supported a higher accuracy of
364 CNN compared to ABC (Fig. S4). Moreover, when the empirical data was evaluated, only
365 CNN recovered two species for the allopatric pair *D. melanogaster-D. sechellia* (Table 2).
366 These results validated our CNN approach, as they are in agreement with our expectations
367 based on Campillo et al. (2020).

368 Regarding the *P. aurisetus* dataset, both CNN and ABC approaches selected the
369 'splitter' model without migration as the most likely scenario with high PP (Table 2). The
370 main difference between CNN and ABC functioning is the ability of the former to take
371 information directly from SNP matrices without using SuSt, which is required by the latter.
372 Moreover, while ABC relies on a rejection step that discards most of the simulations and
373 leaves only a small proportion that are more similar to the empirical data (Csilléry et al.
374 2012), the CNN uses information from the whole set of simulations to learn how to

375 distinguish the concurrent scenarios (Schrider and Kern 2018). The inferior performance of
376 the ABC analyses could also be related to the choice of SuSt with overly high dimensionality
377 (Robert et al. 2011; but see Kousathanas et al. 2016) or with little information to distinguish
378 among the tested models. To reduce dimensionality, we adopted the suggestion of Perez et al.
379 (2016a), which consists of the transformation of the raw SuSt with a PCA and the retention of
380 only the axis necessary to ensure at least 99% of the variance. Other strategies usually applied
381 for this purpose (reviewed in Prangle 2015) include partial least squares regression
382 (Wegmann et al. 2009), linear regression (Fearnhead and Prangle 2012) or boosting
383 (Aeschbacher et al. 2012).

384 Although our CNN results were very encouraging, we note that care must be taken in
385 interpreting them, as deep learning techniques can suffer from overfitting (Nguyen et al.
386 2015; Ponti et al. 2017). To evaluate overfitting, we observed the history plot of the accuracy
387 throughout the epochs (Fig. S3) and adopted a cross-validation approach based on a test set,
388 which consisted of simulated data that were not evaluated during training. The results pointed
389 to high accuracy (Fig. 4 and Fig. S4), which is in agreement with the similarity of our
390 empirical and simulated data (Fig. S5). Another recent approach that could be coupled with
391 our model comparison strategy is based on unsupervised machine learning (Derkarabetian et
392 al. 2019). This strategy showed promising results and was particularly robust in
393 distinguishing population structure from species-level divergence.

394

395 *Delimiting Species in P. aurisetus*

396 *Pilosocereus aurisetus* populations diverged very recently in the last one million years
397 (Perez et al. 2016a). Delimiting species with recent diversification has been considered
398 challenging, and the main difficulty arises from the short time for species to accumulate
399 diagnostic characteristics that allow taxonomic distinction (Salicini et al. 2011). A similar

effect is observed in genetic data and is commonly referred to as incomplete lineage sorting (ILS). ILS appears when ancestral genetic variants persist as polymorphisms across successive diversification events. This phenomenon has been indicated as the primary cause of discordance between gene trees and species trees in Cactaceae (Copetti et al. 2017).

Another issue that imposes additional challenges for species delimitation in *P. aurisetus* is its sky-island distribution, leading to high population divergence (Bonatelli et al. 2014). Topography-driven isolation in species of the Brazilian rupestrian highland habitats ("campos rupestres"), such as *P. aurisetus*, has been considered an important factor driving speciation and high microendemism in these landscapes (Vasconcelos et al. 2020; Zappi et al. 2017). The major concern in this kind of system is that MSC may fail to discriminate between genetic structure associated with population isolation and species boundaries (Jackson et al. 2017; Sukumaran and Knowles 2017; Leaché et al. 2018). Although *gdi* appears as a possible solution for the overspliting tendency of MSC methods (Jackson et al. 2017), mainly in highly structured systems, it is still not clear if it could lead to an opposite effect - over lumping differentiated species. Another possibility for overcoming this bias is to incorporate *a priori* knowledge to determine the structure associated with population-level processes and related to the species level. An ideal scenario would incorporate data from a plethora of classes, such as morphological, ecological, and genetic data, to recover more robust species boundaries (Pinheiro et al. 2018). Since no single method can discriminate between these processes, the results from species delimitation using multispecies coalescent models (MSC) in sky-island systems should be treated as species hypotheses that need further confirmation from multiple sources (Sukumaran and Knowles, 2017).

Taxonomic Implications for P. aurisetus

424 Our species delimitation investigation within *P. aurisetus* is discordant from the
425 currently recognized taxonomic diversity of this taxon (Hunt et al. 2006), as the 'splitter'
426 hypothesis has been recovered with higher probability with different methods. Convergent
427 evolution as well as the level of plasticity commonly found in cactus species (Guerrero et al.
428 2018) might be related to the disagreement in the number of species delimited by current
429 taxonomy and the detected genetic lineages, as observed within the genus *Pilosocereus*
430 (Bonatelli et al. 2014; Perez et al. 2016b). Therefore, our results should provide some
431 guidance for taxonomists interested in re-evaluating the taxonomy of *P. aurisetus*. In this
432 context, our results may help to fill gaps in the traditional taxonomy and provide
433 recommendations for a taxonomic treatment that better reflects the diversity of species,
434 leading us to a multidisciplinary approach for better understanding the boundaries within
435 species complexes considering their evolutionary history.

436 Previous genetic studies have identified well-differentiated lineages within *P. aurisetus*
437 and related species, with monophyletic groups more frequently being associated with the
438 geographic distribution than the proposed taxonomic boundaries (Fig. 2; Bonatelli et al. 2014;
439 Perez et al. 2016b; Calvente et al. 2016; Khan et al. 2018; Lavor et al. 2019). Different
440 taxonomic descriptions have been considered in the past for some of the recovered lineages
441 within *P. aurisetus* that agree with our results. For instance, the populations occurring in the
442 Serra Negra Mountains (ITA and PMN localities), in the center (MEN and INA) and in the
443 northern distribution of the species (EDB and BOV localities) were previously reported as *P.*
444 *aurisetus* subsp. *densilanatus* , *P. aurisetus* subsp. *werdermannianus*, and *P. aurisetus* subsp.
445 *supthutianus* (Braun and Esteves Pereira, 1995), respectively. These subspecies propositions
446 were based on some level of morphological variation that initially seemed rather distinctive,
447 such as the densely wooly stems observed in the ITA populations (Fig. S1). However, Taylor
448 and Zappi (2004) argued that such differences are not sufficiently important to merit

recognition as an additional subspecies. These authors reasoned that if this level of morphological difference was to be recognized, the logical extension would be to give similar status to other populations that show slightly divergent characteristics in terms of size, white-wooly stems, and glaucousness.

CONCLUSIONS

Although the splits within species could be an artifact of the MSC, we might recognize previous taxonomic issues that agree with the inferred species in this investigation. *Pilosocereus aurisetus* exhibits many biological characteristics that make species delimitation challenging, such as recent divergence, a sky-island distribution and unstable taxonomic history. Here, we sought to investigate the species limits in this complex system and, for the first time, incorporated a deep learning approach to select the best species hypothesis according to our data and simulations. Finally, we stress that all the species hypotheses reported here should be considered, as any of the taxonomic species in fact are hypotheses prone to validation with other methods and sources of information.

SUPPLEMENTARY MATERIAL

All scripts and datasets used are available in GitHub: https://github.com/manolofperez/CNN_spDelimitation_Piloso.

FUNDING

This work was supported by grants from the São Paulo Research Foundation (FAPESP) (2015/06160-5 to EMM, 2012/22943-1 to MFP, and 2012/22857-8 to IASB); the National Council for Scientific and Technological Development (CNPq) (03940/2019-0 to EMM,

305301/2018-7 to DCZ); and the Coordination for the Improvement of Higher Education Personnel (CAPES) (Finance Code 001 to MRB).

ACKNOWLEDGMENTS

We thank Heidi Utsunomiya and Juliana de Fátima Martinez for laboratory assistance and Gerardus Olsthoorn and Marlon Machado for sampling assistance.

REFERENCES

Aeschbacher S., Beaumont M.A., Futschik A. 2012. A novel approach for choosing summary statistics in approximate Bayesian computation. Genetics 192:1027–1047.

Alvarado-Sizzo H., Casas A., Parra F., Arreola-Nava H.J., Terrazas T., Sánchez C. 2018. Species delimitation in the *Stenocereus griseus* (Cactaceae) species complex reveals a new species, *S. huastecorum*. PLoS One. 13:e0190385.

Beaumont M.A., Zhang W., Balding D.J. 2002. Approximate Bayesian computation in population genetics. Genetics 162: 2025–2035.

Bonatelli I.A.S., Carstens B.C., Moraes E.M. 2015. Using next generation RAD sequencing to isolate multispecies microsatellites for *Pilosocereus* (Cactaceae). PLoS One. 10:e0142602.

Bonatelli I.A.S., Perez M.F., Townsend A.P., Taylor N.P., Zappi D.C., Machado M.C., Koch I., Pires A.H.C., Moraes E.M. 2014. Interglacial microrefugia and diversification of a cactus species complex: Phylogeography and palaeodistributional reconstructions for *Pilosocereus aurisetus* and allies. Mol. Ecol. 23:3044-3063.

Bouckaert R., Heled J., Kühnert D., Vaughan T., Wu C.H., Xie D., Suchard M.A., Rambaut A., Drummond A.J. 2014. BEAST 2: a software platform for Bayesian evolutionary analysis. PLoS Comput. Biol. 104:e1003537.

498 Braun P.J., Esteves Pereira E. 1995. Nieuwe combinaties en namen voor cactussen uit
499 Brazilië, Bolivia en Paraguay. Succulenta (Netherlands). 74: 134-135.
500 Carstens B.C., Pelletier T.A., Reid N.M., Satler J.D. 2013. How to fail at species
501 delimitation? Mol. Ecol. 22:4369–4383.
502 Calvente A., Moraes E.M., Lavor P., Bonatelli I.A.S., Nacaguma P., Versieux L.M., Taylor
503 N.P., Zappi D.C. 2017. Phylogenetic analyses of *Pilosocereus* (Cactaceae) inferred from
504 plastid and nuclear sequences. Bot. J. Linn. Soc. 183:25–38.
505 Camargo A., Morando M., Avila L.J., Sites Jr J.W. 2012. Species delimitation with ABC and
506 other coalescent-based methods: a test of accuracy with simulations and an empirical
507 example with lizards of the *Liolaemus darwinii* complex (Squamata: Liolaemidae).
508 Evolution 66:2834-2849.
509 Campillo, L.C., Barley, A.J., Thomson, R.C. 2020. Model-based species delimitation: are
510 coalescent species reproductively isolated? Syst. Biol. 69(4):708-721.
511 Copetti D., Búrquez A., Bustamante E., Charboneau J.L.M., Childs K.L., Eguiarte L.E., Lee
512 S., Liu T.L., McMahong M.M., Whiteman N.K., Winga R.A, Wojciechowskii M.F.,
513 Sanderson M.J. 2017. Extensive gene tree discordance and hemiplasy shaped the
514 genomes of North American columnar cacti. Proc. Natl. Acad. Sci. U S A. 114:12003-
515 12008.
516 Csilléry K., François O., Blum M.G.B. 2012. abc: an R package for approximate Bayesian
517 computation (ABC). Methods Ecol. Evol. 3:475–479.
518 de Queiroz K. 2007. Species concepts and species delimitation. Syst. Biol. 56: 879–886.
519 Denham S.S., Brignonea N.F., Johnson L.A., Pozner R.E. 2019. Using integrative taxonomy
520 and multispecies coalescent models for phylogeny reconstruction and species
521 delimitation within the "Nastanthus–Gamocarpha" clade (Calyceraceae). Mol.
522 Phylogenet. Evol. 130:211-226.

Derkarabetian S., Castillo S., Koo P.K., Ovchinnikov S., Hedin M. 2019. A demonstration of unsupervised machine learning in species delimitation. Mol. Phylogenet. Evol. 139:106562.

Domingos F.M., Bosque R.J., Cassimiro J., Colli G.R., Rodrigues M.T., Santos M.G., Beheregaray L.B. 2014. Out of the deep: Cryptic speciation in a Neotropical gecko (Squamata, Phyllodactylidae) revealed by species delimitation methods. Mol. Phylogenet. Evol. 80:113–124.

Drummond A.J., Rambaut A. 2007. BEAST: Bayesian evolutionary analysis by sampling trees. BMC Evol. Biol. 7:214.

Ence D.D., Carstens B.C. 2011. SpedeSTEM: a rapid and accurate method for species delimitation. Mol. Ecol. Resour. 11:473–480.

Fearnhead P., Prangle D. 2012. Constructing summary statistics for approximate Bayesian computation: Semi-automatic ABC. J. R. Statist. Soc. B. 74:419–474.

da Fonseca E.M., Colli G.R., Werneck F.P., Carstens B.C. 2020. Phylogeographic model selection using convolutional neural networks. bioRxiv.2020.09.11.291856.

Flagel L., Brandvain Y., Schrider D.R. 2019. The unreasonable effectiveness of convolutional neural networks in population genetic inference. Mol. Biol. Evol. 36:220-238

Guerrero P.C., Majure L.C., Cornejo-Romero A., Hernández-Hernández T. 2018. Phylogenetic relationships and evolutionary trends in the Cactus family. J. Hered. 110:4–21.

Guillot G., Mortier F., Estoup A. 2005. GENELAND: a computer package for landscape genetics. Mol. Ecol. Resour. 5:712–715.

546 Harvey M.G., Smith B.T., Glenn T.C., Faircloth B.C., Brumfield R.T. 2016. Sequence
547 capture versus restriction site associated DNA sequencing for shallow systematics. Syst.
548 Biol. 65:910–924.
549 Hernández-Hernández T., Hernández H.M., Arturo De-Nova J., Puente R., Eguiarte L.E.,
550 Magallón S. 2011. Phylogenetic relationships and evolution of growth form in Cactaceae
551 (Caryophyllales, Eudicotyledoneae). Am. J. Bot. 98:44–61.
552 Hunt D., Taylor N.P., Charles G. 2006. The new Cactus Lexicon: Atlas & Text. dh Books,
553 Milborne Port.
554 Jackson N.D., Carstens B.C., Morales A.E., O'Meara B.C. 2017. Species delimitation with
555 gene flow. Syst. Biol. 66:799–812.
556 Katoh K., Standley D. M. 2013. MAFFT multiple sequence alignment software version 7:
557 improvements in performance and usability. Mol. Biol. Evol. 30:772–780.
558 Khan G., Godoy M.O., Franco F.F., Perez M.F., Taylor N.P., Zappi D.Z., Machado M.C.,
559 Moraes E.M. 2018. Extreme population subdivision or cryptic speciation in the cactus
560 *Pilosocereus jauruensis*? A taxonomic challenge posed by a naturally fragmented
561 system. Syst. Biodivers. 16:188–199.
562 Kousathanas A., Leuenberger C., Helfer J., Quinodoz M., Foll M., Wegmann D. 2016.
563 Likelihood-Free Inference in High-Dimensional Models. Genetics 203:893–904.
564 Lanfear R., Calcott B., Ho S.Y., Guindon S. 2012. PartitionFinder: combined selection of
565 partitioning schemes and substitution models for phylogenetic analyses. Mol. Biol. Evol.
566 29(6): 1695-1701.
567 Lavor P., Calvente A., Versieux L. M., Sanmartin I. 2019. Bayesian spatio-temporal
568 reconstruction reveals rapid diversification and Pleistocene range expansion in the
569 widespread columnar cactus *Pilosocereus*. J. Biogeogr. 46:238–250.

570 Leaché, A.D., Fujita, M.K., Minin, V.N., Bouckaert, R.R. (2014). Species delimitation using
571 genome-wide SNP data. Syst. Biol. 63(4): 534-542.
572 Leaché A.D., Zhu T., Rannala B., Yang Z. 2018. The spectre of too many species. Syst. Biol.
573 68:168–181.
574 Li H. 2013. Aligning sequence reads, clone sequences and assembly contigs with BWA-
575 MEM. arXiv 1303.3997.
576 Li H., Handsaker B., Wysoker A., Fennell T., Ruan J., Homer N., Math G., Abecasis G.,
577 Durbin R. 2009. The sequence alignment/map format and SAMtools. Bioinformatics
578 25:2078–2079.
579 Luo A., Ling C., Ho S.Y.W., Zhu C. 2018. Comparison of methods for molecular species
580 delimitation across a range of speciation scenarios. Syst. Biol. 67:830–846.
581 Martin M. 2011. Cutadapt removes adapter sequences from high-throughput sequencing
582 reads. EMBnet. Journal 17:10–12.
583 McGuire G., Wright F. 2000. TOPAL 2.0: improved detection of mosaic sequences within
584 multiple alignments. Bioinformatics 16:130–134.
585 McKenna A., Hanna M., Banks E., Sivachenko A., Cibulskis K., Kernytsky A., Garimella K.,
586 Altshuler D., Gabriel S., Daly M., DePristo M.A. 2010. The Genome Analysis Toolkit: a
587 MapReduce framework for analyzing next-generation DNA sequencing data. Genome
588 Res. 20:1297–1303.
589 Milne I., Lindner D., Bayer M., Husmeier D., McGuire G., Marshall D.F., Wright F. 2008.
590 TOPALi v2: a rich graphical interface for evolutionary analyses of multiple alignments
591 on HPC clusters and multi-core desktops. Bioinformatics 25:126–127.
592 Morales A.E., Jackson N.D., Dewey T.A., O'Meara B.C., Carstens B.C. 2017 Speciation with
593 gene flow in North American Myotis bats. Syst. Biol. 66:440–452.

Nguyen A.,Yosinski J., Clune J. 2015. Deep neural networks are easily fooled: High confidence predictions for unrecognizable images. In IEEE Conference on Computer Vision and Pattern Recognition (CVPR), p. 427–436.

Oliveira, E.A.D., Perez, M.F., Bertollo, L.A.C., Gestich, C.C., Ráb, P., Ezaz, T., Souza, F.H.S., Viana, P., Feldberg, E., Oliveira, E.H.C.D., Cioffi, M.B., 2020. Historical demography and climate driven distributional changes in a widespread Neotropical freshwater species with high economic importance. Ecography 43: 1291-1304.

Pei J., Chong C., Xin L., Bin L., Yufeng W. 2018. CLADES: A classification-based machine learning method for species delimitation from population genetic data. Mol. Ecol. Resour. 18:1144–1156.

Perez M.F., Bonatelli I.A.S., Moraes E.M, Carstens B.C. 2016a. Model-based analysis supports interglacial refugia over long-dispersal events in the diversification of two South American cactus species. Heredity 116:550–557.

Perez M.F., Carstens B.C., Rodrigues G.L., Moraes E.M., 2016b. Anonymous nuclear markers reveal taxonomic incongruence and long-term disjunction in a cactus species complex with continental-island distribution in South America. Mol. Phylogenetics Evol. 95: 11-19.

Perez M.F., Carstens B.C., Rodrigues G.L., Moraes E.M. 2016c. Anonymous nuclear markers data supporting species tree phylogeny and divergence time estimates in a cactus species complex in South America. Data Brief 6:456–460.

Petkova D., Novembre J., Stephens, M. 2016. Visualizing spatial population structure with estimated effective migration surfaces. Nat. Genet. 48:94–100.

Pinheiro F., Dantas-Queiroz M.V., Palma-Silva C. 2018. Plant Species Complexes as Models to Understand Speciation and Evolution: A Review of South American Studies. Crit. Rev. Plant Sci. 37:54–80.

Ponti M., Ribeiro L., Nazare T., Bui T., Collomosse J. "Everything you wanted to know about Deep Learning for Computer Vision but were afraid to ask". In: 30th SIBGRAPI Conference on Graphics, Patterns and Images Tutorials (SIBGRAPI-T), 17–41. IEEE.

Prangle, D. 2015. Summary statistics in approximate Bayesian computation. arXiv preprint arXiv:1512.05633.

Rambaut A., Suchard M.A., Xie D., Drummond A.J. 2014. Tracer v1.6. Available from: URL http://beast.bio.ed.ac.uk/Tracer.

Rannala B., Yang Z. 2020. *Species Delimitation*. In: Scornavacca C., Delsuc F., Galtier, N. Phylogenetics in the Genomic Era. No commercial publisher | Authors open access book, 5.5:1–18. ffhal-02536468

Robert C.P., Cornuet J.M., Marin J.M., Pillai N.S. 2011. Lack of confidence in approximate Bayesian computation model choice. Proc. Natl Acad. Sci. U S A. 108:15112–15117.

Rosenberg N.A. 2004. DISTRUCT: a program for the graphical display of population structure. Mol Ecol Notes. 4:137–138.

Salicini I., Ibáñez C., Juste J. 2011. Multilocus phylogeny and species delimitation within the Natterer's bat species complex in the Western Palearctic. Mol. Phylogenet. Evol. 61:888–898.

Sanchez, T., Cury, J., Charpiat, G., Jay, F. 2020. Deep learning for population size history inference: Design, comparison and combination with approximate Bayesian computation. Mol. Ecol. Resour. 00: 1– 16.

Souza, F.H.S., Perez, M.F., Bertollo, L.A.C., Oliveira, E.A., Lavoué, S., Gestich, C.C., Ráb, P., Ezaz, T., Liehr, T., Viana, P.F., Feldberg, E., Cioffi, M.B. 2019. Interspecific Genetic

Differences and Historical Demography in South American Arowanas (Osteoglossiformes, Osteoglossidae, *Osteoglossum*). Genes 10: 693.

Sukumaran J., Knowles L.L. 2017. Multispecies coalescent delimits structure, not species. Proc. Natl Acad. Sci. U S A. 114:1607–1612.

Schrider D.R., Kern A.D. 2018. Supervised Machine Learning for Population Genetics: A New Paradigm. Trends Genet. 34:301–312.

Smith M.L., Carstens B.C. 2020. Disentangling the process of speciation using machine learning. Evolution 74:216-229.

Solís-Lemus C., Knowles L.L., Ané C. 2015. Bayesian species delimitation combining multiple genes and traits in a unified framework. Evolution 69:492–507.

Taylor N.P., Zappi D.C. 2004. Cacti of Eastern Brazil. Royal Botanic Gardens, Kew.

Untergrasser A., Cutcutache I., Koressaar T., Ye J., Faircloth B.C., Remm M., Rozen S.G. 2012. Primer3 – new capabilities and interfaces. Nucleic Acids Res. 40: e115.

Vasconcelos T.N.C., Alcantara S., Andrino C.O., Forest F., Reginato M., Simon M.F., Pirani J.R. 2020. Fast diversification through a mosaic of evolutionary histories characterizes the endemic flora of ancient Neotropical mountains. Proc. R. Soc. B 287: 20192933.Wegmann D., Leuenberger C., Excoffier L. 2009. Efficient approximate Bayesian computation coupled with Markov chain Monte Carlo without likelihood. Genetics 182:1207–1218.

Weyenberg G., Huggins P.M., Schardl C.L., Howe D.K., Yoshida R. 2014. kdetrees: non-parametric estimation of phylogenetic tree distributions. Bioinformatics 30:2280–2287.

Yang Z., Rannala B. 2014. Unguided species delimitation using DNA sequence data from multiple loci. Mol. Biol. Evol. 31:3125–3135.

Zappi D.C.1994. *Pilosocereus* (Cactaceae). The Genus in Brazil. Royal Botanic Gardens, Kew.

667 Zappi D.C., Moro M.F., Meagher T.R., Lughadha E.N. 2017. Plant biodiversity drivers in
668 Brazilian campos rupestres: insights from phylogenetic structure. Front. Plant. Sci.
669 8:2141.

670

671 FIGURE CAPTIONS

672 FIGURE 1. A general protocol for species delimitation in *P. aurisetus*, comparing the adopted
673 CNN and ABC approaches. (1) Evaluate delimitation hypotheses based on taxonomic and
674 genetic information with the BPP (Yang and Rannala 2014); (2) simulate genetic data for
675 each delimitation hypothesis, with and without gene flow among lineages (+M models); (3)
676 transform the simulated data for the two approaches, CNN (convert to images, with black
677 pixels representing the major and white pixels representing the minor frequency alleles for
678 each segregating site) and ABC (extract SuSt averaged over loci); (4) train a neural network
679 (CNN) to recognize simulations generated from each model; (5) use independent simulations
680 to evaluate and compare the accuracy of CNN and ABC; (6) predict model probability, with
681 the trained network for the CNN approach or by approximating the posterior (retaining only
682 the 20% most similar simulations) for ABC.

683

684 FIGURE 2. (A) Geographic distribution of the sampled localities and elevational range in
685 eastern Brazil (codes according to Table 1). Symbols (triangles and circle) represent the
686 currently recognized *P. aurisetus* subspecies, and gray shades represent heterotypic
687 synonyms of *P. aurisetus* subsp. *aurisetus* (in parenthesis). The delimited species are shown
688 with lines colored according to the delimited entities in Fig. 3.

689

690 FIGURE 3. Species delimitation results are represented as bars at the tips of the topology
691 obtained in BPP. Values in parentheses above each bar present the number of species for each

692 hypothesis. The numbers at the nodes represent Beast PP/BPP ‘specific’/and ‘diffuse’ prior
693 values. Symbols (triangles and circles) represent both currently recognized and synonymized
694 (in parenthesis) *P. aurisetus* taxa. A representative of each inferred species is shown, next to
695 the limits according to the 'splitter' hypothesis.
696
697 FIGURE 4. Cross-validation test to compare the performance of different model comparison
698 methods (CNN - filled lines and ABC - dashed lines) and numbers of simulations. Each point
699 represents the probability of choosing the "correct" model (i.e., the model from which the
700 data were simulated) over incorrect models. Each color represents a different scenario,
701 including (+M) or not migration between the OTUs.
702
703 APPENDICES
704 SUPPLEMENTARY FILE 1. Detailed simulation and model selection methods.
705
706 SUPPLEMENTARY TABLE S1. Primer sequence of each marker used in this study for
707 microfluidic amplification. The genomic region for each marker is coded as follows: nr =
708 nuclear, mt = mitochondrial, and cp = plastidial. Substitution models are provided for loci
709 used in the final analyses.
710
711 SUPPLEMENTARY FIGURE S1. Representatives of *P. aurisetus* subsp. *aurisetus* (A-D), and *P.*
712 *aurisetus* subsp. *aurilanatus* (E) sampled in this study. A. *P. aurisetus* subsp. *aurisetus*; B.
713 syn. *P. aurisetus* subsp. *werdermannianus*; C. syn. *P. aurisetus* subsp. *densilanatus*; D. syn.
714 *P. aurisetus* subsp. *supthutianus*; E. *P. aurisetus* subsp. *aurilanatus*. Photo credit: EMM.
715

716 SUPPLEMENTARY FIGURE S2. Posterior distribution of genealogical divergence index (*gdi*)
717 values generated by the BPP analysis. Color scheme according to branches from the tree
718 depicted in the upper right corner, with locality names following Fig. 2.
719
720 SUPPLEMENTARY FIGURE S3. Accuracy of the CNN along the training epochs with varying
721 numbers of simulations (500 in orange, 1,000 in yellow and 10,000 in green) for the training
722 (filled lines) and validation (dashed lines) sets.
723
724 SUPPLEMENTARY FIGURE S4. Confusion matrices showing the percentage of predicted classes
725 for each simulated scenario (model representation for *P. aurisetus* following Fig. 1) using test
726 data (independent simulations not evaluated in the training step). The results are shown for
727 both methods (CNN and ABC) in the three taxonomic systems analyzed (*P. aurisetus* and the
728 species pais *D. melanogaster-D. simulans* and *D. melanogaster-D. sechellia*.
729
730 SUPPLEMENTARY FIGURE S5. Principal coordinate analysis for simulated and empirical data in
731 *P. aurisetus*. Simulations from the 'splitter' model are shown following the same color
732 scheme in Fig. 1.
733

Table 1. Sampling localities for *P. aurisetus* and their assignment to operational taxonomic units according to three different species delimitation hypotheses ('splitter', 'lumper', 'BPP_noGDI' and 'BPP_GDI').

Taxon/Locality	Code	N	Longitude	Latitude	Delimitation hypothesis			
					'splitter'	'lumper'	'BPP_noGDI'	'BPP_GDI'
P. a. subsp. *aurisetus*								
Cocais-MG	COC	4	-43,450000	-19,866667	1	1	1	1
Itamarandiba-MG (a)	ITA	4	-42,935972	-18,001944	2	1	2	1
Pedra Menina-MG (a)	PMN	4	-43,044500	-18,136250	2	1	2	1
Olhos D'Água-MG (b)	ODA	4	-43,622361	-17,438833	3	1	3	1
Engenheiro Dolabela-MG (b)	EDB	4	-43,793667	-17,451417	3	1	3	1
Bocaiúva-MG (b)	BOV	4	-43,755833	-17,545833	3	1	3	1
Mendanha-MG (c)	MEN	4	-43,536583	-18,118917	4	1	2	1
Inhaí-MG (c)	INA	4	-43,605833	-17,146444	4	1	2	1
P. a. subsp. *aurilanatus*								
Joaquim Felício-MG	JFE	4	-44,178333	-17,757833	5	2	4	1

(a), (b) and (c) indicate the samples from the previously synonymized forms *P. a.* subsp. *densilanatus*, *P. a.* subsp. *supthutianus* and *P. a.* subsp. *werdermannianus*, respectively.

Table 2. Model selection results for *P. aurisetus* and the two *Drosophila* species pairs using empirical data. CNN values are softmax probabilities for each scenario, while posterior probabilities are shown for ABC. The scenario with the highest probability for each method is shown in bold.

Scenario	CNN	ABC
P. aurisetus		
Splitter	**0.998**	**0.994**
Splitter+Migration	0.001	0.000
Lumper	0.000	0.000
Lumper+Migration	0.000	0.000
BPP+GDI	0.000	0.000
BPP_noGDI	0.001	0.006
BPP_noGDI+Migration	0.000	0.000
D. melanogaster_D.simulans		
One Species	0.008	0.018
Two Species	**0.992**	**0.982**
D. melanogaster_D. sechellia		
One Species	0.051	**0.894**
Two Species	**0.949**	0.106

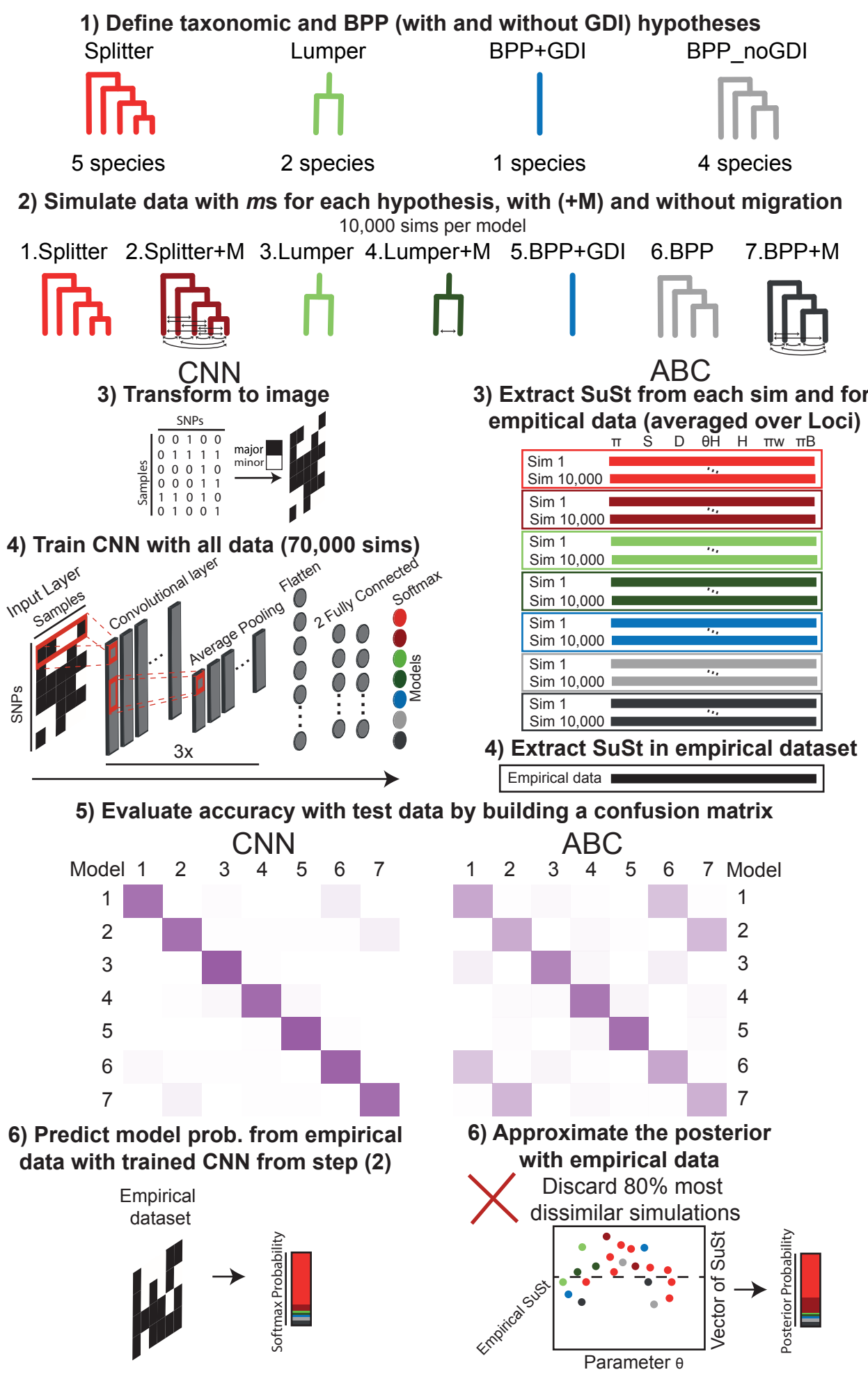
1) Define taxonomic and BPP (with and without GDI) hypotheses
Splitter
Lumper
BPP+GDI
BPP_noGDI
5 species
2 species
1 species
4 species
2) Simulate data with ms for each hypothesis, with (+M) and without migration
10,000 sims per model
1.Splitter
2.Splitter+M
3.Lumper
4.Lumper+M
5.BPP+GDI
6.BPP
7.BPP+M
CNN
ABC
3) Transform to image
SNPs
Samples
major
minor
3) Extract SuSt from each sim and for empirical data (averaged over Loci)
π S D θH H πw πB
Sim 1
Sim 10,000
4) Train CNN with all data (70,000 sims)
Input Layer
Samples
SNPs
Convolutional layer
Average Pooling
Flatten
2 Fully Connected
Softmax
Models
3x
4) Extract SuSt in empirical dataset
Empirical data
5) Evaluate accuracy with test data by building a confusion matrix
CNN
ABC
Model
1 2 3 4 5 6 7
6) Predict model prob. from empirical data with trained CNN from step (2)
Empirical dataset
Softmax Probability
6) Approximate the posterior with empirical data
Discard 80% most dissimilar simulations
Empirical SuSt
Vector of SuSt
Parameter θ
Posterior Probability

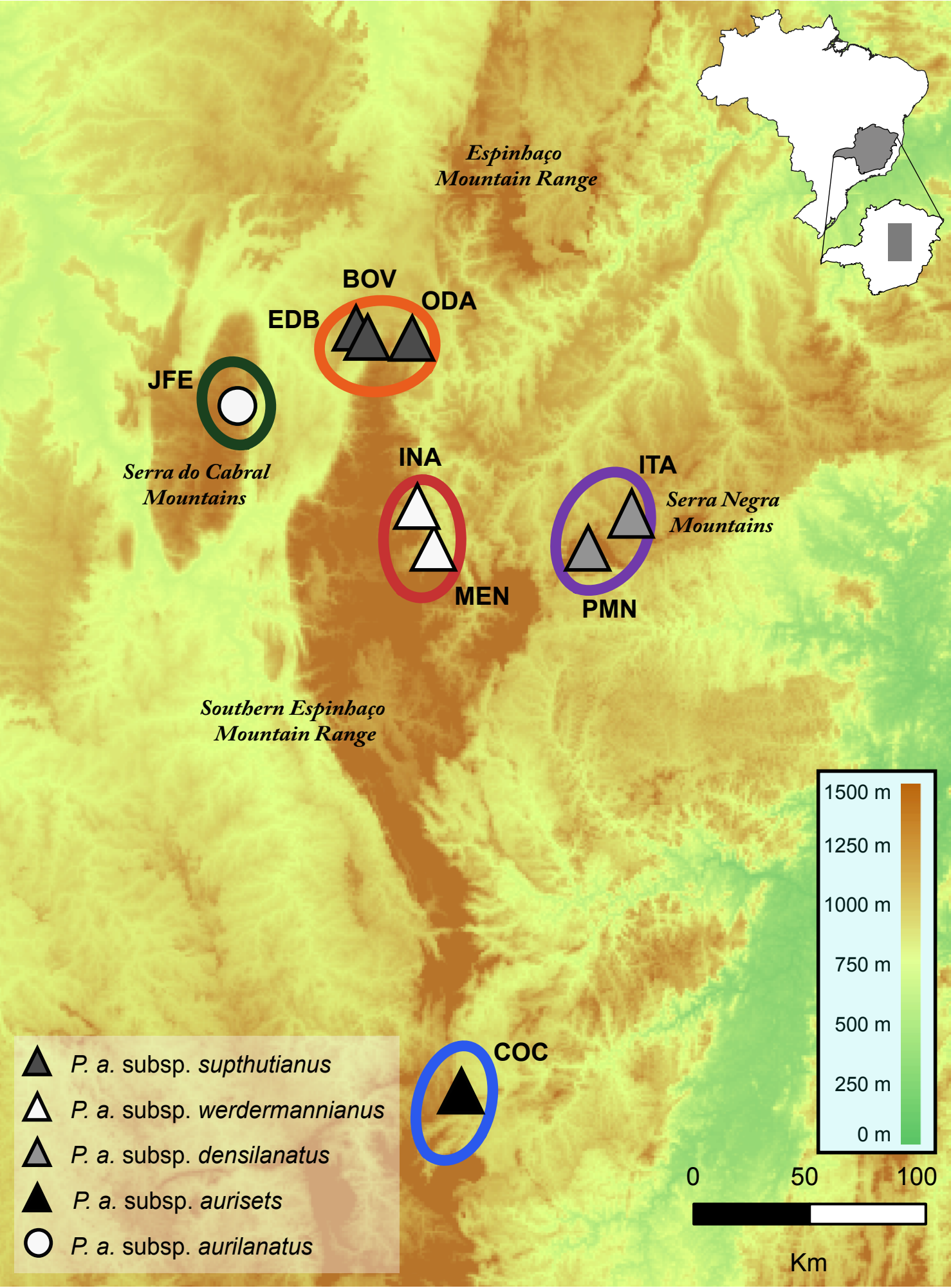
Espinhaço
Mountain Range
BOV
ODA
EDB
JFE
Serra do Cabral
Mountains
INA
MEN
ITA
Serra Negra
Mountains
PMN
Southern Espinhaço
Mountain Range
COC
1500 m
1250 m
1000 m
750 m
500 m
250 m
0 m
0
50
100
Km
P. a. subsp. supthutianus
P. a. subsp. werdermannianus
P. a. subsp. densilanatus
P. a. subsp. aurisets
P. a. subsp. aurilanatus

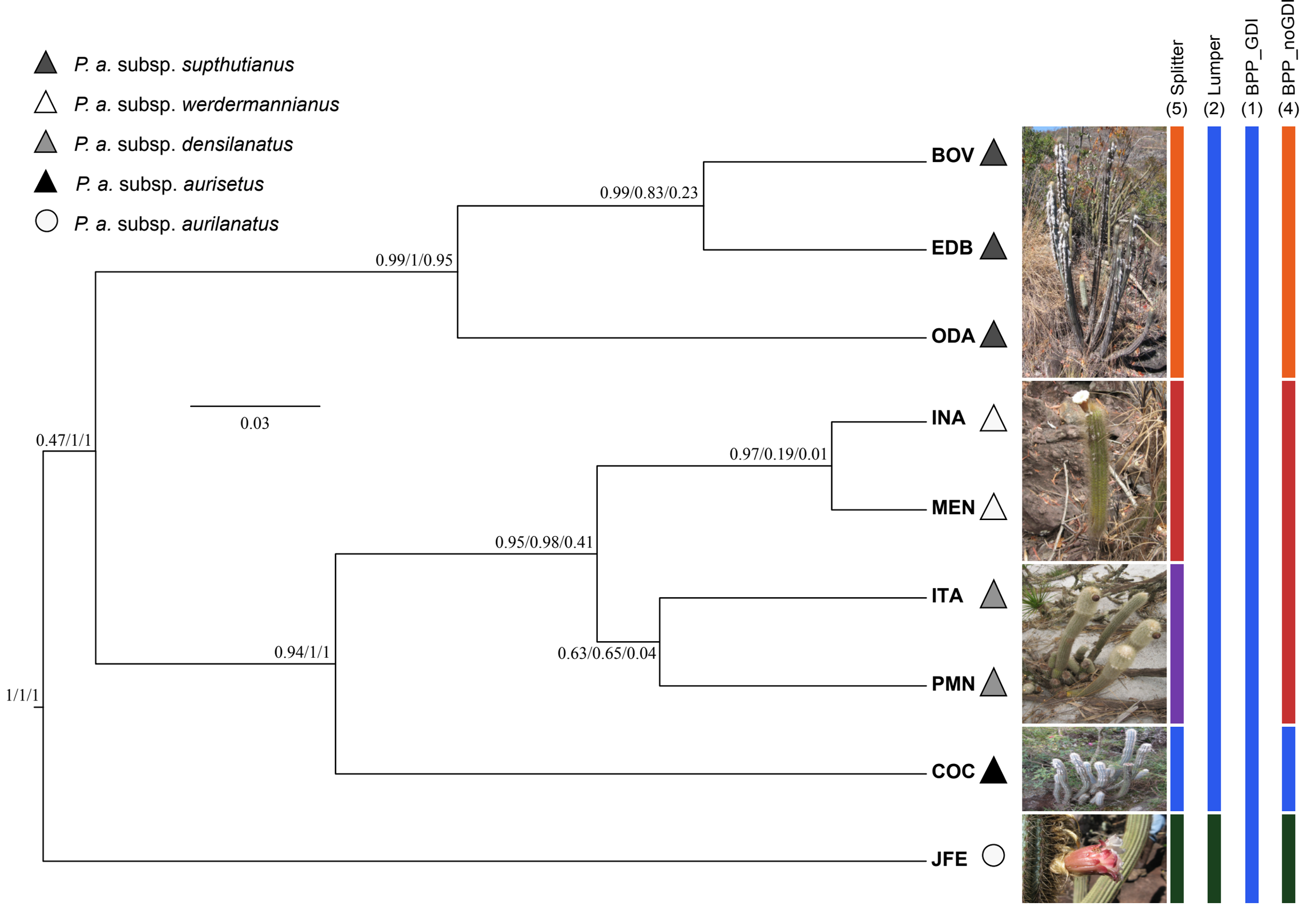
P. a. subsp. supthutianus
P. a. subsp. werdermannianus
P. a. subsp. densilanatus
P. a. subsp. aurisetus
P. a. subsp. aurilanatus
Splitter (5)
Lumper (2)
BPP_GDI (1)
BPP_noGDI (4)
BOV
EDB
ODA
INA
MEN
ITA
PMN
COC
JFE
0.99/0.83/0.23
0.99/1/0.95
0.03
0.47/1/1
0.97/0.19/0.01
0.95/0.98/0.41
0.63/0.65/0.04
0.94/1/1
1/1/1

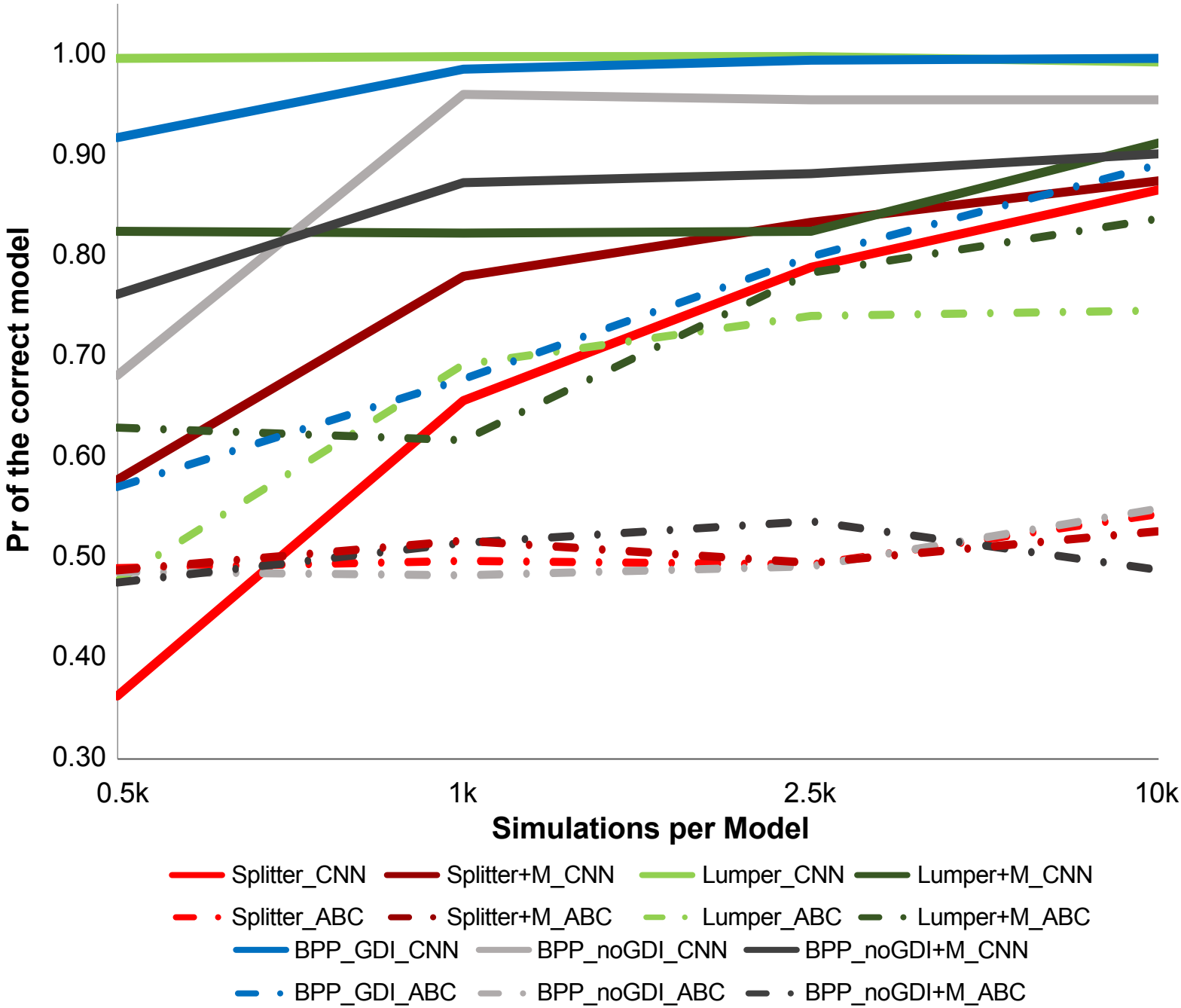
1.00
0.90
0.80
0.70
0.60
0.50
0.40
0.30
Pr of the correct model
0.5k
1k
2.5k
10k
Simulations per Model
Splitter_CNN
Splitter+M_CNN
Lumper_CNN
Lumper+M_CNN
Splitter_ABC
Splitter+M_ABC
Lumper_ABC
Lumper+M_ABC
BPP_GDI_CNN
BPP_noGDI_CNN
BPP_noGDI+M_CNN
BPP_GDI_ABC
BPP_noGDI_ABC
BPP_noGDI+M_ABC